

Diagrammatic Quantum Monte Carlo for Two-Body Problem: Exciton

E. A. Burovski¹, A. S. Mishchenko^{2,1}, N. V. Prokof'ev³, and B. V. Svistunov¹

¹*RRC 'Kurchatov Institute', 123182, Moscow, Russia*

²*Correlated Electron Research Center, Tsukuba Central 4, Tsukuba 305-8562, Japan*

³*Department of Physics, University of Massachusetts, Amherst, Massachusetts 01003*

We present a novel method for precise numerical solution of the irreducible two-body problem and apply it to excitons in solids. The approach is based on the Monte Carlo simulation of the two-body Green function specified by Feynman's diagrammatic expansion. Our method does not rely on the specific form of the electron and hole dispersion laws and is valid for any attractive electron-hole potential. We establish limits of validity of the Wannier (large radius) and Frenkel (small radius) approximations, present accurate data for the intermediate radius excitons, and give evidence for the charge transfer nature of the monopolar exciton in mixed valence materials.

PACS numbers: 71.53.-y, 02.70.Ss, 05.10.Ln

After it was realized that under certain conditions the electron dynamics in conduction band is of two-particle nature due to Coulomb attraction to the hole in the valence band left behind [1], the problem of exciton became a model example of an irreducible (center-of-mass motion does not separate from the rest of degrees of freedom) two-body problem. The simplest (still rather general) exciton Hamiltonian [2,3] consists of conduction and valence band contributions, H_0 , and coupling H_{e-h} :

$$H_0 = \sum_{\mathbf{k}} \varepsilon_c(\mathbf{k}) e_{\mathbf{k}}^\dagger e_{\mathbf{k}} + \sum_{\mathbf{k}} \varepsilon_v(\mathbf{k}) h_{\mathbf{k}} h_{\mathbf{k}}^\dagger, \quad (1)$$

$$H_{e-h} = -N^{-1} \sum_{\mathbf{p}, \mathbf{k}, \mathbf{k}'} \mathcal{U}(\mathbf{p}, \mathbf{k}, \mathbf{k}') e_{\mathbf{p}+\mathbf{k}}^\dagger h_{\mathbf{p}-\mathbf{k}}^\dagger h_{\mathbf{p}-\mathbf{k}'} h_{\mathbf{p}+\mathbf{k}'}. \quad (2)$$

Here $e_{\mathbf{k}}$ ($h_{\mathbf{k}}$) is the electron (hole) annihilation operator, $\varepsilon_c(\mathbf{k})$ ($\varepsilon_v(\mathbf{k})$) is the conduction (valence) band dispersion law, N is the number of lattice sites, and $\mathcal{U}(\mathbf{p}, \mathbf{k}, \mathbf{k}')$ is an attractive interaction potential.

Despite numerous efforts over the years there is no rigorous technique to solve for exciton properties even for the simplest model given above which treats electron-electron interactions as a static renormalized Coulomb potential with averaged dynamical screening. The only solvable cases are the Frenkel small-radius limit [1] and the Wannier large-radius limit [4] which describe molecular crystals and wide gap insulators with large dielectric constant, respectively. Much more frequently encountered cases of intermediate radius excitons (e.g. intermediate gap semiconductors, LiF, or mixed valence systems) have to be dealt with using approximate numerical approaches. There are powerful *ab initio* modern methods [5–7] for band structure and effective electron-hole potential calculations, but the real bottleneck is in numerical solution of the two-particle problem for a bulk material. One can either solve the Bethe-Salpeter equation on a finite mesh in reciprocal/direct space [5–7], or employ the random-phase approximation decoupling [2]. However, both methods suffer from systematic errors, and

the Bethe-Salpeter equation on finite mesh may lead to incorrect eigenstates for the Wannier case [7]. Therefore, even the limits of validity of the Wannier and Frenkel approximations can not be established by existing methods.

Besides, an efficient and rigorous method for the study of exciton properties, given the band structure, is of high virtue for phenomenological models. As an example, we refer to the protracted discussion of numerous (and often contradictory) models concerning exciton properties in mixed valence semiconductors [8]. In Ref. [9] unusual properties of SmS and SmB₆ were explained by invoking the excitonic instability mechanism assuming charge-transfer nature of the optically forbidden exciton. Although this model explains quantitatively the phonon spectra [10], optical properties [11,12], and magnetic neutron scattering data [13], its basic assumption has been criticized as being groundless [14].

In this Letter we describe how ground state properties of excitons in the model (1)-(2) can be obtained numerically without systematic errors for arbitrary dispersion relations $\varepsilon_c(\mathbf{k})$ and $\varepsilon_v(\mathbf{k})$, and attractive potential $\mathcal{U}(\mathbf{p}, \mathbf{k}, \mathbf{k}')$. First, we show that the problem fits into the diagrammatic Monte Carlo (MC) method [15–17] which sums positively-definite perturbation series, in our case Feynman diagrams, for the two-particle Matsubara Green function, G . We then describe the procedure of extracting various physical properties from the asymptotic long-time behavior of G . Next, we discuss our results for a particular tight-binding model and electron-hole interaction potential to see under what conditions Frenkel and Wannier approximations remain accurate. Finally, we present evidence that the band structure of mixed valence materials results in the charge-transfer character of the optically forbidden exciton.

The two-particle Green function with total momentum $2\mathbf{p}$ in imaginary time representation is defined as

$$G_{\mathbf{p}}^{\mathbf{k}\mathbf{k}'}(\tau) = \langle 0 | e_{\mathbf{p}+\mathbf{k}'}(\tau) h_{\mathbf{p}-\mathbf{k}'}(\tau) h_{\mathbf{p}-\mathbf{k}}^\dagger e_{\mathbf{p}+\mathbf{k}}^\dagger | 0 \rangle, \quad (3)$$

where the vacuum state $| 0 \rangle$ corresponds to empty

conduction and filled valence bands, and $h_{\mathbf{p}-\mathbf{k}}(\tau) = e^{H\tau}h_{\mathbf{p}-\mathbf{k}}e^{-H\tau}$, $\tau > 0$. In the interaction representation G can be written as a sum of ladder-type Feynman diagrams, see Fig. 1: pairs of horizontal solid lines represent free electron-hole pair propagators, $G_{\mathbf{p}}^{(0)}(\mathbf{k}, \tau_2 - \tau_1) = \exp(-\varepsilon(\mathbf{k})(\tau_2 - \tau_1))$, where $\varepsilon(\mathbf{k}) = \varepsilon_c(\mathbf{p} + \mathbf{k}) - \varepsilon_v(\mathbf{p} - \mathbf{k})$ is the energy of the pair, and dashed lines represent the interaction potential. For purely numerical rea-

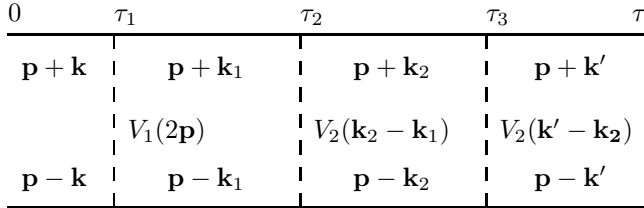


FIG. 1. A typical diagram contributing to $G_{\mathbf{p}}^{\mathbf{k}\mathbf{k}'}(\tau)$.

sons explained below we split the potential into two terms $\mathcal{U}(\mathbf{p}, \mathbf{k}, \mathbf{k}') = V_1(2\mathbf{p}) + V_2(\mathbf{k} - \mathbf{k}_1)$, and expand in both V_1 and V_2 . [This can be done because [2] $\mathcal{U}(\mathbf{p}, \mathbf{k}, \mathbf{k}') = V_0 - W(2\mathbf{p}) + U(\mathbf{k} - \mathbf{k}')$ where V_0 is the on-site coupling, $W(2\mathbf{p})$ is the dipolar term, $U(\mathbf{k} - \mathbf{k}') = \sum_{\lambda \neq 0} \exp(i\mathbf{q}\mathbf{R}_\lambda) / (R_\lambda \epsilon(\mathbf{R}_\lambda))$ is the monopolar term, and $\epsilon(\mathbf{R}_\lambda)$ is a static dielectric screening function (we set the electric charge to unity). Since $U(\mathbf{q})$ is not positive definite [in fact $\sum_{\mathbf{q}} U(\mathbf{q}) = 0$] we add and subtract some constant \bar{U} to ensure that $V_1(2\mathbf{p}) = V_0 - W(2\mathbf{p}) - \bar{U}$ and $V_2(\mathbf{q}) = \bar{U} + U(\mathbf{q})$ are both positive - this imposes the only limitation on value V_0 in our method].

The final answer for G is given by the sum of all possible diagrams. Formally we can write this as a series of multi-dimensional integrals

$$G_{\mathbf{p}}^{\mathbf{k}\mathbf{k}'}(\tau) = \sum_{m=0}^{\infty} \sum_{\xi_m} \int dx_1 \cdots dx_m F_{\mathbf{p}}^{\mathbf{k}\mathbf{k}'}(\tau; \xi_m; x_1, \dots, x_m).$$

where x_1, \dots, x_m are internal variables [times and momenta, $x_i = (\tau_i, \mathbf{k}_i)$] of the m -th order diagram, the summation over ξ_m accounts for different diagrams of order m , and the “weight” F is given by the product of electron-hole propagators and interaction vertices according to standard rules. For positive V_1 and V_2 all terms in the series are positive definite and one may apply the diagrammatic Monte Carlo technique developed in Refs. [15,16], which evaluates such series without systematic errors (by Metropolis-type sampling of diagrams according to their weight directly in the momentum-time continuum). Since the method itself is well described in the literature we will concentrate on the problem specific details only.

The crucial for the whole scheme update is the one which changes the number of interaction vertices by one. To render algorithm efficient one has to propose new internal parameters as close

as possible to the distribution function $R(x_{m+1}) = F(\xi_{m+1}; x_1, \dots, x_m, x_{m+1}) / F(\xi_m; x_1, \dots, x_m)$ defined by the ratio of the new and old diagram weights. This is done in order to maximize the acceptance ratio P_{acc} — if proposed $x_{m+1} = (\tau_{m+1}, \mathbf{k}_{m+1})$ are distributed according to some normalized function $W(x_{m+1})$, then $P_{\text{acc}} \propto R(x_{m+1}) / W(x_{m+1})$. Otherwise the choice of $W(x_{m+1})$ is a matter of computational convenience [15,16].

First, we select (with equal probabilities) which interaction vertex, V_1 or V_2 , will be inserted, and then select at random the time interval where it will be placed, $\tau_{m+1} \in (\tau_a, \tau_b)$, where $\tau_{a,b}$ are the interval boundaries determined either by the existing interaction vertices or the diagram ends. All the momenta at $\tau < \tau_a$ and $\tau > \tau_{m+1}$ are kept untouched. In case when $V_1(2\mathbf{p})$ is inserted, the new momentum \mathbf{k}_{m+1} is proposed uniformly in the Brillouin zone (BZ). When $V_2(\mathbf{k}_b - \mathbf{k}_{m+1})$ is inserted (\mathbf{k}_b is the relative motion momentum to the left of point (τ_b) the new momentum \mathbf{k}_{m+1} is proposed using distribution function $W(\mathbf{k}_{m+1}) = (\beta/2\pi \arctan \beta)^3 \prod_{\alpha} \left(1 + \beta k_{m+1}^{(\alpha)} / \pi\right)^{-1}$, where $\alpha = x, y, z$. The parameter β is uniformly seeded on interval $[\beta_{\min}, \beta_{\max}]$ at each step, and $\beta_{\min}, \beta_{\max}$ are further tuned to maximize the acceptance ratio. We note, that different distribution functions used to propose new momentum \mathbf{k}_{m+1} when dealing with V_1 and V_2 vertices was the only motivation behind an artificial separation $\mathcal{U} = V_1 + V_2$ [The actual gain in efficiency was about three orders of magnitude!]. Finally, the time position for the new vertex was seeded according to the distribution function dictated by the diagram weights ratio $W(\tau_{m+1}) = \delta\epsilon \cdot e^{-\delta\epsilon\tau_{m+1}} / (e^{-\delta\epsilon\tau_a} - e^{-\delta\epsilon\tau_b})$ where, $\delta\epsilon = \varepsilon(\mathbf{k}_{m+1}) - \varepsilon(\mathbf{k}_b)$.

We also employ standard Metropolis updates changing the values of internal momenta and times, which substantially enhances the efficiency of the algorithm.

We now turn to the discussion of how exciton properties are obtained from the $G(\tau \rightarrow \infty)$ limit. An eigenstate $|\nu; \mathbf{p}\rangle$ with energy E_ν can be written as

$$|\nu; \mathbf{p}\rangle \equiv \sum_{\mathbf{k}} \xi_{\mathbf{p}\mathbf{k}}(\nu) e_{\mathbf{p}+\mathbf{k}}^\dagger h_{\mathbf{p}-\mathbf{k}}^\dagger |0\rangle. \quad (4)$$

where amplitudes $\xi_{\mathbf{p}\mathbf{k}}(\nu) = \langle \nu; \mathbf{p} | e_{\mathbf{p}+\mathbf{k}}^\dagger h_{\mathbf{p}-\mathbf{k}}^\dagger | 0 \rangle$ describe the wave function of internal motion of the exciton. In terms of exciton eigenstates we have, $G_{\mathbf{p}}^{\mathbf{k}=\mathbf{k}'}(\tau) = \sum_{\nu} |\xi_{\mathbf{p}\mathbf{k}}(\nu)|^2 e^{-E_\nu\tau}$, and if τ is much larger than inverse energy difference between the ground and first excited states, the Green function projects to the ground state, $G_{\mathbf{p}}^{\mathbf{k}=\mathbf{k}'}(\tau \rightarrow \infty) = |\xi_{\mathbf{p}\mathbf{k}}(\text{g.s.})|^2 e^{-E_{\text{g.s.}}\tau}$. Due to normalization condition $\sum_{\mathbf{k}} |\xi_{\mathbf{p}\mathbf{k}}(\nu)|^2 \equiv 1$ the asymptotic behavior of the sum $\tilde{G}_{\mathbf{p}} = \sum_{\mathbf{k}} G_{\mathbf{p}}^{\mathbf{k}=\mathbf{k}'}$ is especially simple, $\tilde{G}(\tau) \rightarrow e^{-E_{\text{g.s.}}\tau}$. This asymptotic behavior allows simulations of energy and amplitudes at fixed τ [large enough to make the corresponding systematic error negligible], using the technique of Monte Carlo estimators.

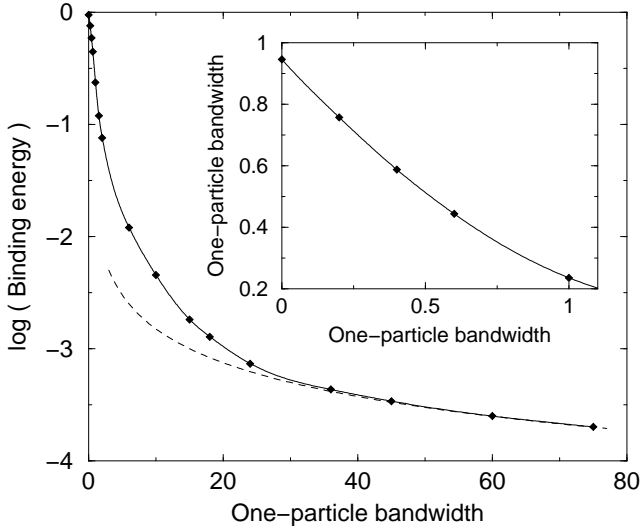


FIG. 2. The dependence of the exciton binding energy on the bandwidth $E_c = E_v$. Statistical errors are less than $5 \cdot 10^{-3}$ in relative units. The dashed line corresponds to the Wannier model. The solid line is the cubic spline, the derivatives at the right and left ends being fixed by the Wannier limit and perturbation theory, respectively. Insert: the initial part of the plot.

To this end we differentiate each diagram for $\tilde{G}(\tau)$ [18] with respect to τ and arrive at the result (compare with Ref. [16])

$$E_{\text{g.s.}} = \tau^{-1} \left\langle \sum_{j=1}^{m+1} \varepsilon^j(\mathbf{k}) \Delta\tau_j - m \right\rangle_{\text{MC}}, \quad (5)$$

where $\langle \dots \rangle_{\text{MC}}$ stands for the MC statistical average, m is the diagram order, $\varepsilon^j(\mathbf{k})$ and $\Delta\tau_j$ are the electron-hole pair energy and duration of the j -th propagator, respectively. By definition, in the limit $\tau \rightarrow \infty$ we have $G_{\mathbf{p}}^{\mathbf{k}=\mathbf{k}'} / \tilde{G}_{\mathbf{p}} = |\xi_{\mathbf{p}\mathbf{k}}(\text{g.s.})|^2$, i.e. the distribution over quasimomentum \mathbf{k} is related to the wave function of internal motion. The wave function of the bound state can be chosen real, and the Fourier transform may be used to obtain $|\text{g.s.}\rangle$ in direct space [19].

In this Letter we focus on the study of exciton properties in a simple cubic 3D lattice with tight binding dispersion laws for the electron and hole bands

$$\varepsilon_{c,v}(\mathbf{k}) = \tilde{E}_{c,v} \pm (E_{c,v}/6) \sum_{\alpha} (1 - \cos k_{\alpha}). \quad (6)$$

The choice of interaction parameters was motivated by the possibility to cover all regimes (from Wannier to Frenkel limit) by varying the ratio between the bandwidth and the gap only. Our simulations were done for $\tilde{E}_v = 0$, $E_g \equiv \tilde{E}_c = 1$, $W(2\mathbf{p} = 0) = -0.168$, $V_0 = 0.778$, $\bar{U} = 0.578$, and $\epsilon(\mathbf{R}) = 10$ [20]. The binding energy in the Frenkel limit E_{FL} ($E_{c,v} \ll E_g$) is then less than the gap, $E_{\text{FL}} = V_1(2\mathbf{p} = 0) + \sum_{\mathbf{q}} V_2(\mathbf{q}) = 0.946$, thus rendering the exciton stability for all values of $E_{c,v}$. In the

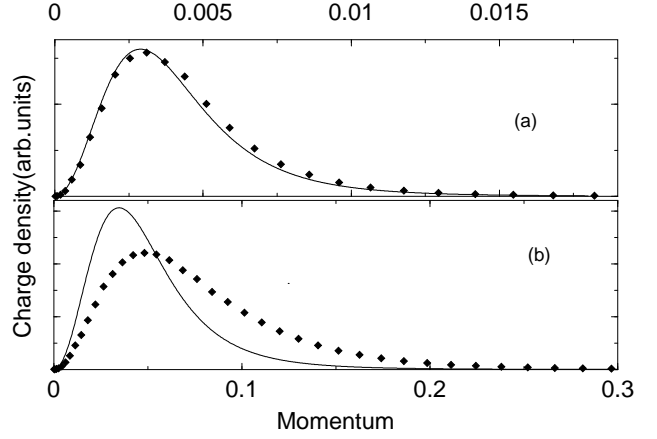


FIG. 3. The momentum dependence of the charge density $|\xi_{\mathbf{p}\mathbf{k}}(\text{g.s.})|^2 k^2$ for $E_c = E_v = 60$ (a) and $E_c = E_v = 10$ (b). Solid lines are the Wannier model result. Statistical errors are typically of order 10^{-4} .

Wannier limit of large bandwidth $E_{c,v} \gg E_g$ the binding energy approaches $3/(2\epsilon^2 E_c)$ (assuming $E_v = E_c$). Of course, our parameters satisfy the requirement that V_1 and V_2 are positive definite functions.

Our results for the binding energy and wave function are shown in Figs. 2, 3, and 4. First we notice that the method works equally well in all regimes, and statistical errors are much smaller than symbols sizes in all plots. An unexpected result is that extremely large bandwidth $E_c/E_g > 20$ is necessary for the Wannier approximation to be adequate: both the binding energy E_B (Fig. 2) and the wave function [21] (Fig. 3 and Fig. 4 (b)) demonstrate large deviations for smaller E_c/E_g . Most surprisingly, for $1 < E_c/E_g < 10$ the wave function has a large (and dominating) on-site component [Fig. 4(b)], but the binding energy is not even close to the Frenkel limit! For $E_c/E_g = 0.4$ the wave function is almost entirely localized [Fig. 4(c)] but $E_{\text{g.s.}}$ is still 50% away from the small-radius limit. Noticing that $E_{\text{g.s.}} \approx E_{\text{FL}} - (E_c + E_v)/2$ ($E_c = E_v$), which holds for localised functions when $E_c < 0.4$, we deduce that the deviation from Frenkel result is determined by the electron and hole delocalization energy. Our conclusion is then that the intermediate-range regime is very broad and relevant in most practical cases.

To study the structure of optically forbidden excitons in mixed valence compounds we choose typical for these semiconducting materials band spectra [8], i.e. an almost flat valence band separated by an indirect gap from the wide conduction band with maximum at $\mathbf{k} = 0$ and minimum at the BZ boundary. One can see in Fig. 5 that this leads to the charge transfer character of the optically forbidden monopolar exciton ($W(2\mathbf{p}) = 0$) when the wave function of internal motion has almost zero on-site component, maximal charge density at near neighbours, and large long-ranged oscillations at neighboring sites. The

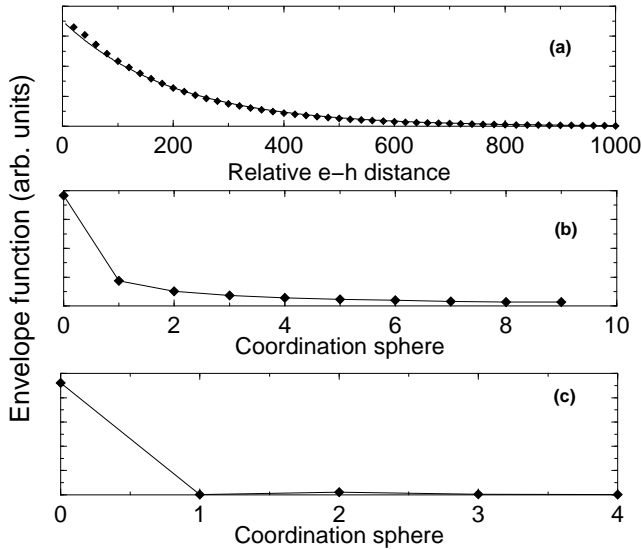


FIG. 4. The wave function of internal motion in real space: (a) Wannier [$E_c = E_v = 60$]; (b) intermediate [$E_c = E_v = 10$]; (c) near-Frenkel [$E_c = E_v = 0.4$] regimes. The solid line in the panel (a) is the Wannier model result while solid lines in other panels are to guide an eye only. Statistical errorbars are of order 10^{-4} .

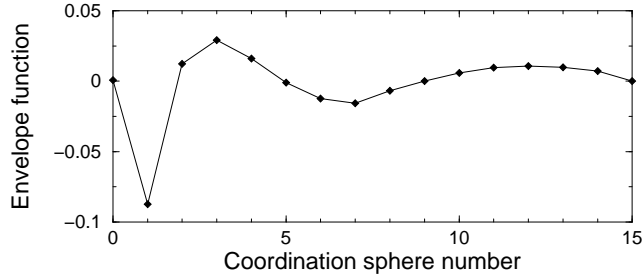


FIG. 5. The wave function of internal motion in real space for the optically forbidden monopolar ($W(2\mathbf{p}) = 0$) exciton defined by the following model parameters: $\tilde{E}_c = 1.5$, $\tilde{E}_v = 0$, $E_c = -0.5$, $E_v = 0.05$, $\epsilon = 10$, $V_0 = 0.578$. Statistical errorbars are of order 10^{-4} .

difference with the previously discussed $E_{v,c}/E_g = 0.4$ case, see Fig. 4(b), is remarkable.

Finally, we would like to note that diagrammatic MC technique not only gives properties of the ground state but is also suitable for the study of excited states and optical absorption [22]. This can be done by simulating the τ dependence of $\mathcal{G}(\mathbf{p} = \mathbf{0}, \tau) = \sum_{\mathbf{k}\mathbf{k}'} G_{\mathbf{p}=0}^{\mathbf{k}\mathbf{k}'}(\tau)$, and solving numerically equation

$$\mathcal{G}(\mathbf{p} = \mathbf{0}, \tau) = \int_0^\infty g(\omega) \exp(-\omega\tau) d\omega$$

to obtain the spectral function $g(\omega)$ [16].

We thank A. Sakamoto and N. Nagaosa for fruitful discussions. We acknowledge the support of the National Science Foundation under Grant DMR-0071767 and RFBR grant 01-02-16508.

-
- [1] J. I. Frenkel, Phys. Rev. **17**, 17 (1931).
 - [2] I. Egri, Phys. Reports **119**, 364 (1985).
 - [3] R. Knox, Theory of excitons, (Academic press, New York 1963).
 - [4] J. H. Wannier, Phys. Rev. **52**, 191 (1937).
 - [5] S. Albrecht, L. Reining, R. D. Sole, and G. Onida, Phys. Rev. Lett. **80**, 4510 (1998).
 - [6] L. X. Benedict, E. L. Shirley, and R. B. Bohn, Phys. Rev. Lett. **80**, 4514 (1998).
 - [7] M. Rohlfing and S. G. Louie, Phys. Rev. Lett. **81**, 2312 (1998).
 - [8] S. Curnoe and K. A. Kikoin, Phys. Rev. B **61** 15714 (2000);
 - [9] K. A. Kikoin and A. S. Mishchenko, J. Phys.: Condens. Matter, **2**, 6491 (1990).
 - [10] A. S. Mishchenko and K. A. Kikoin, J. Phys.: Condens. Matter, **3**, 5937 (1991).
 - [11] G. Travaglini and P. Wachter, Phys. Rev. B **29**, 893 (1984).
 - [12] P. Lemmens, A. Hoffmann, A. S. Mishchenko, M. Yu. Talantov, and G. Güntherodt, Physica B **206&207**, 371 (1995).
 - [13] K. A. Kikoin and A. S. Mishchenko, J. Phys.: Condens. Matter, **7**, 307 (1995);
 - [14] T. Kasuya, Europhys. Lett., **26**, 277 (1994); T. Kasuya, Europhys. Lett., **26**, 283 (1994)
 - [15] N. V. Prokof'ev and B. V. Svistunov, Phys. Rev. Lett. **81**, 2514 (1998).
 - [16] A. S. Mishchenko, N. V. Prokof'ev, A. Sakamoto, and B. V. Svistunov, Phys. Rev. B **62**, 6317 (2000).
 - [17] A. S. Mishchenko and N. Nagaosa, Phys. Rev. Lett. **86**, 4624 (2001).
 - [18] Working with the function \tilde{G} introduces a certain formal problem: the zero- and first-order (with respect to $V_2(\mathbf{q} = 0)$) diagrams contain macroscopically large factor N . Being interested in the ground-state properties only, we can safely omit them, since explicit analysis shows that they are irrelevant in the $\tau \rightarrow \infty$ limit.
 - [19] If the quantity $|\xi_{\mathbf{p}\mathbf{k}}(\text{g.s.})|^2$ has no nodes, the amplitudes $\xi_{\mathbf{p}\mathbf{k}}(\text{g.s.})$ can be chosen positive. Since $G_{\mathbf{p}}^{\mathbf{k}\mathbf{k}'}(\tau)$ is given by the sum of positive-definite diagrams we know that $\xi_{\mathbf{p}\mathbf{k}}(\text{g.s.})$ has no nodes.
 - [20] The direct coupling term was evaluated by generalized Evald method, see e.g. M. H. Cohen and F. Keffer, Phys. Rev. **99**, 1128 (1955).
 - [21] While for Wannier regime the wave function is spherically symmetric, it's symmetry for the Frenkel and intermediate case regimes bears the lattice structure thus making the coordination spheres number a natural unit for the representation of the wave function in direct space.
 - [22] In the case when the interband optical matrix element is momentum independent, the absorption coefficient is proportional to $g(\omega)$.